IIUC Studies, Vol.-20, Issue-1, June 2023
DOI: https://doi.org/10.3329/iiucs.v20i1.69053

Path loss and group delay investigation for in-human body to on-human body transmission using dipole and loop antenna

Md. Ismail Haque
Department of Electrical & Electronic Engineering
International Islamic University Chittagong (IIUC), Bangladesh

Abstract
The most critical aspects for a successful transceiver design for wireless body area communication system are path loss and group delay investigation of the human body. In this research, we used a 150 mm length dipole and 40 mm diameter loop antenna to analyze path loss and group delay at 10-60 MHz HBC band for implant communication. An anatomical human body model in the near field constituency was used with FDTD simulations to build the path loss model. For a small dipole antenna, the path loss increases by an exponent of 6.62 with distance, especially along the height direction of the body, and the average group delay is in the order of 1ns. On the other hand, the average group delay is less than 1 ns and the path loss grows by an exponent of 4.65 for a loop antenna. Finally, it is demonstrated that both antennas have good accuracy and have no effect on data speeds below 20 Mbps but the loop antenna has a better overall performance in this investigation.

Keywords FDTD simulation, implant channel, path loss, group delay.

Paper type Research paper

1. Introduction

Wireless body area communication technology is progressing rapidly which is great strides and innovative advances in tiny electronic devices. Wireless body area networks (WBAN) (Haque, Wang, & Anzai, 2019) have been identified as advantageous for medical services and healthcare applications (Wang, 2012; Haque, Yamada, Shi, Wang, & Anzai, 2021; Haque, Wang, & Anzai, 2019; Haque, Yoshibayashi, Wang, Fischer, & Kirchner, 2021). WBAN connects nodes on or in a person's body, and it has revolutionized patient monitoring and healthcare facilities (Haque, Yoshibayashi, Wang, & Anzai, 2021; Haque, Yamamoto, Wang, & Kakimoto, 2022; Wang, Liu, Suguri, & Anzai, 2015; Wang, 2020; Peng, Saito, & Ito, 2018; Yuce, & Dissanayake, 2012). Active implants in the human body allow to improve the patient's quality of life through better and faster diagnosis. A robust wireless

IIUC Studies
Vol.-20, Issue-1, June 2023
pp. 121-140

ISSN 2408-8544

communication channel, a high data rate for real-time transmission, and low power consumption are requirements for a medical application to assure the longevity of the device (Wang & Wang, 2012). The development of an endoscope capsule system (Wang, 2020) is a typical example of implant communication. It allows investigation of parts of the small intestine that are not accessible with other endoscopes. The advantages of using a capsule endoscope for better diagnosis are evident. Furthermore, because this surgery does not include any wires or tubes, the patient's comfort is enhanced.

Capsule endoscopes transmit images by using the "medical implant communication service (MICS) band" (Wang, 2020). However, the transmission bandwidth in the 400 MHz MICS spectrum is severely constrained to 300 kHz (Haque, Wang, & Anzai, 2019). "Ultra wide band (UWB) low-band" (Peng, Saito, & Ito, 2018) communication, in contrast to the MICS band results in high transmission, but the UWB signal suffers from severe attenuation when it goes through the human body. Consequently, the UWB low-band reduces the accuracy of implant communication. These problems can be resolved using the industrial, scientific, and medical (ISM) band, however there is no safeguard against interference from other communication services using the same band. By considering the above circumstances, the use of the HBC (10–60 MHz) band presents a plethora of possibilities for this wireless link to satisfy the aforementioned requirements (Yuce, & Dissanayake, 2012). Some path loss (PL) models for wireless implant communications were studied at 400 MHz (Anzai, Katsu, Chavez-Santiago, Wang, Plettemeier, Wang, & Balasingham, 2014), 900 MHz (Wang, Nomura, Narita, Ito, Anzai, Bergsland, & Balasingham, 2018), and UWB (Lopez-Linares Roman, Vermeeren, Thielens, Joseph, & Martens, 2014). However, there has been no research about path loss and group delay features within or outside the human body for channel modeling in the 10-60 MHz HBC band. We all know that wave propagation in a person's body is quite challenging. The lossy dielectric characteristics of body tissues in the human body cause absorption and the heterogeneous structure of body tissues cause scattering (Wang & Wang, 2012). As a result, the transmitted signal is greatly weakened. Diffractions and creeping waves also exist along the body's surface, generating shadow fading in the shadowed zones. Furthermore, the human body is made up of a range of postures and different body organs could travel during communication. As a result, several routes are generated between the transmitter and receiver. Therefore, a received signal may be made up of several attenuated, delayed, time-varying, and distorted copies of the transmitted signal. Due to body postures and

motions, an on-body channel may experience greater multipath fading and shadowing than an in-body channel, while an in-body channel has more severe signal degradation during transmission inside the body than an on-body channel. In a body area network, channel modeling combines wave propagation, path loss, and group delay features.

In order to investigate path loss and group delay in the 10–60 MHz HBC (Human Body Communication) band, the goal of this research is to create a channel using a tiny dipole and loop antenna. FDTD numerical simulations and an anatomical human body model are used to create the channel model from the scratch. The path loss model is then created and the results compared using dipole and loop antennas. Finally, the group delay influence of the in-body to on-body (IB2OB) shadowing channel is explored using both antennas for wide band pulse excitation at 35 MHz. This study supports the viability of a capsule endoscope as well as additional medical implant body area network (BAN) linkages. The novelty of this research is to investigate path loss and group delay for In-Human Body to On-Human Body (IHB2OHB) transmission using dipole and loop antenna as a part of channel modeling.

2. Analysis method and human modeling

In this study, we employed anatomical human body models as a simulation tool for our research. Here, SEMCAD software was used as simulation tool. Figures 1 and 2 show the simulation of a human body's environment with a tiny dipole antenna on its surface to capture capsule endoscope data. The human body model is composed of a sophisticated anatomical configuration with over 51 types of tissue and a spatial precision of 2 mm (Shinoda, Anzai, & Wang, 2017; Shi, Anzai, & Wang, 2012; Nagaoka, Watanabe, Saurai, Kunieda, Watanabe, Taki, & Yamanaka, 2004). Gabriel's data is largely used in the database on the dielectric characteristics of biological tissue (Gabriel, 1996). For the bellow anatomical model, the dielectric properties were used separately for path loss analysis in the frequency range of 10- 60 MHz and at center frequency 35 MHz for group delay investigation respectively. The actual capsule endoscope system is designed so that the transmitting antenna is located inside the body and the receiving antenna is located outside the body. To make simulation easier, we decided to make the transmitting antenna a 150-mm and 40-mm long z-directed dipole on the body surface, and a 150-mm and 40-mm diameter loop on the body surface, respectively, with 45 edge sensors for the dipole antenna and 45 current sensors for the loop antenna in the small intestine to take 15 locations and three directions.

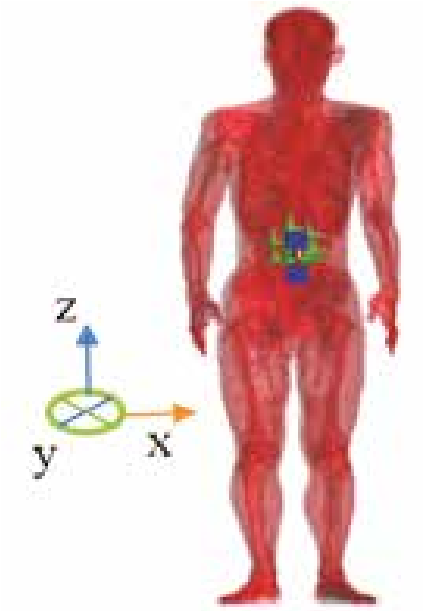

Figure 1
FDTD simulation environment with dipole antenna geometry with labeling

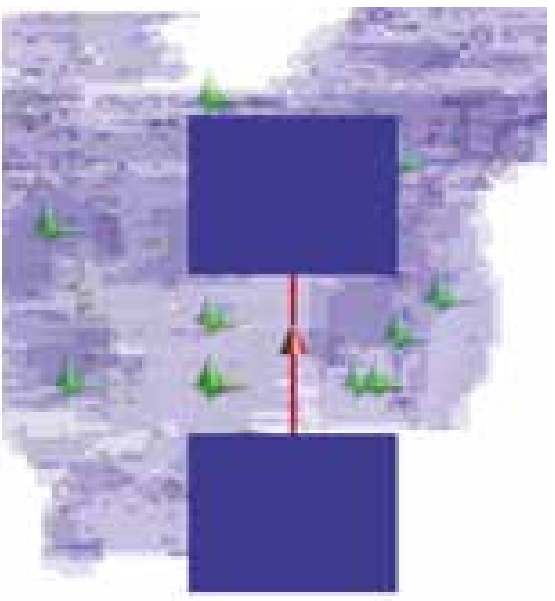

Figure 2
Geometry arrangement of transmitting dipole antenna in small intestine

The simulation environments in Figures 3 and 4 show a human body with a little loop antenna on its surface for receiving capsule endoscope data. The length of each receiving antenna was set at 10 mm. 45 edge sensors for dipole antenna and 45 current sensors for loop antenna were put within the body at the polarization directions x, y, and z based on realistic movement rotations of the capsule endoscope. As a result, we obtained 45 data points at the in-body location for extracting propagation channel characteristics. The path loss analysis was carried out in the harmonic simulation setup, with varied relative permittivity and electrical conductivity at frequencies ranging from 10 to 60 MHz, using the finite difference time domain (FDTD) approach in conjunction with the anatomical human body model.

Additionally, for the group delay analysis, we used a broadband simulation setting and a pulse sending signal.

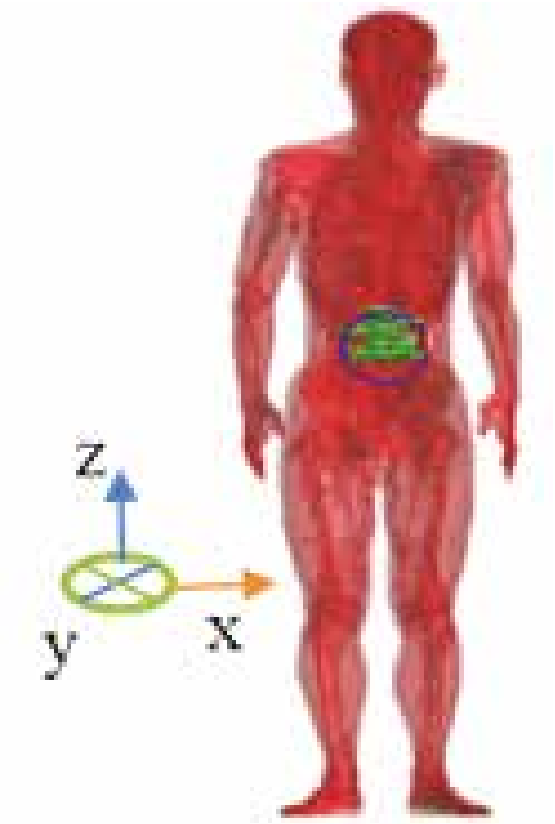

Figure 3
FDTD simulation environment with loop antenna geometry with labeling

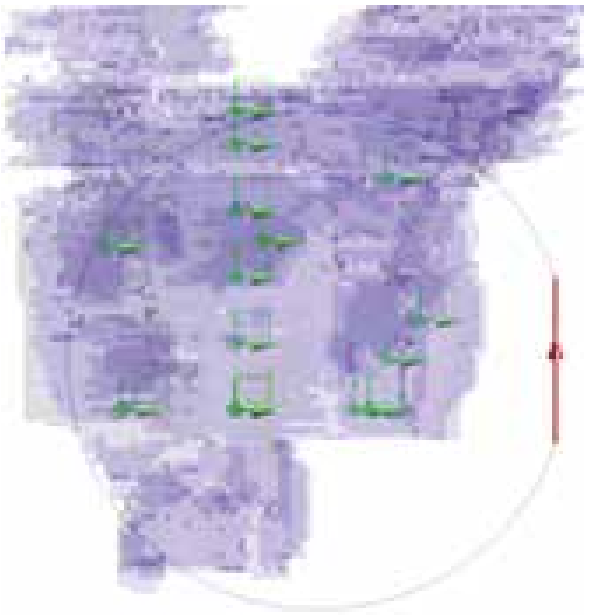

Figure 4
Geometry arrangement of transmitting loop antenna in small intestine

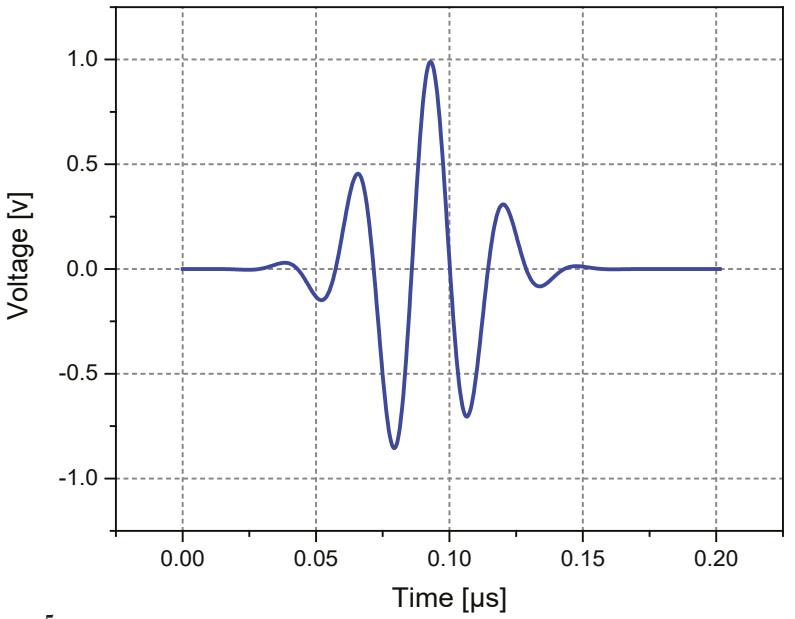

Figure 5
Dipole antenna's time waveform of transmitted signal

Figures 5 and 6 depict the time waveform and frequency spectrum of the dipole antenna's transmitted pulse signal, respectively when dipole antenna was excited by 1 V edge source; and they agreed well and the reflection coefficient S_{11} was found as high as 0.97. The produced peak voltage was found to be around 1 V at around 0.09 μs as shown in time domain waveform. The maximum peak voltages were observed around at 40 MHz. The maximum peak voltage was found around 78 V as shown in frequency domain waveform.

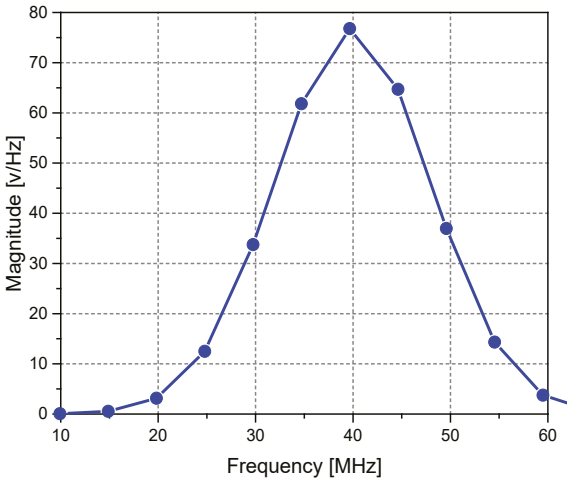

Figure 6
Dipole antenna's frequency spectrum of transmitted signal

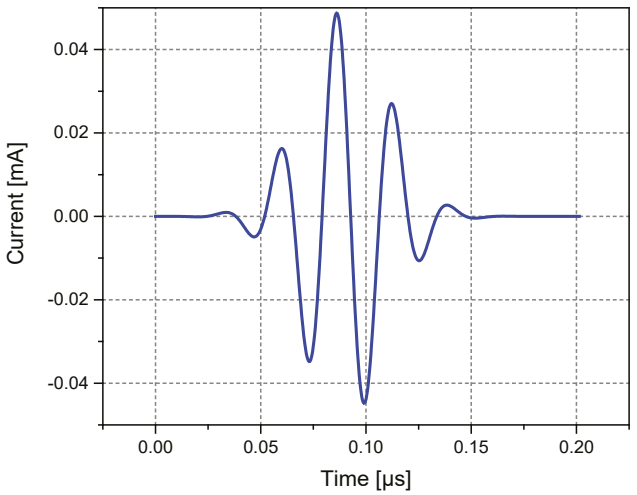

Figure 7
Loop antenna's time waveform of transmitted signal

The time waveform and frequency spectrum of the transmitted signal for the loop antenna are shown in Figures 7 and 8, respectively when the excitation magnitude was investigated by current; and the reflection coefficient $S_{11}$was found as 0. 95 which is low compared to dipole antenna. The produced peak current was found to be around 0.045 mA at around 0.08 μs as shown in time domain waveform. The maximum peak currents were observed around at 35 MHz. The maximum peak current was found around 3.55 mA as shown in frequency domain waveform.

3. Path Loss modeling results and discussion

After getting FDTD simulation results, we computed the transmitting power P_t as well as the receiving power P_r at various frequency (10-60 MHz) respectively. Path loss is defined in our calculation by taking the distance *d* from the transmitting antenna T_x and the receiving antenna R_x by the following:

$$PL_{dB,d} = 10log_{10}[\frac{P_t}{P_r}] \quad (1)$$

The "path loss in dB at a given distance d" (Haque, Wang, & Anzai, 2019) can be modeled by the dependent equation below, which includes shadowing and is specified by an empirical power decay rule function as:

$$PL_{dB,d} = PL_{dB,d_0} + 10nlog_{10}\left[\frac{P_t}{P_r}\right] + S_{dB} \quad (2)$$

where d is the distance between the in-body receiver and the on-body transmitter, d_0 is the reference distance (10 mm), and the path loss exponent n is determined by the environment through which the RF (radio frequency) signal travels. For example, everyone knows that n=2 at free space. But a significantly higher path loss exponent value can be found due to the human body's lossy environment. S_{dB} is referred to as shadowing or random scatter about the mean path loss and refers to dB deviation caused by various organs (e.g., skin, lungs, bone, muscle, liver, kidney, hearth, etc.) nearby the transmitter and antenna gain in different directions.

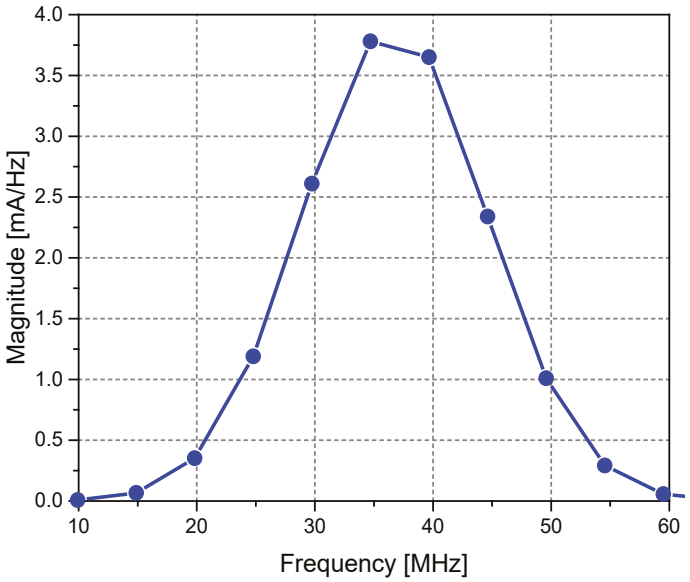

Figure 8
Loop antenna's frequency spectrum of transmitted signal

The average for path loss (PL) at each location from 10 to 60 MHz for obtaining a frequency-band-averaged PL*(d)* as a function of distance *d* was investigated. All path losses in dB from 10 to 60 MHz band at x, y and z directions were calculated. At 10-60 MHz, two scenarios were investigated while both the transmitting and receiving antennas were z-directed. One as shown in Figure 9 is dipole antenna, and other one as shown in Figure 10 is for loop antenna. The average path loss (APL) at 10-60 MHz was calculated as follows for each in-body to on-body link:

$$\mathrm{APL} = 10log_{10}[\frac{PL_{10}+PL_{20}+PL_{30}+PL_{35}+PL_{40}+PL_{50}+PL_{60}}{7}] \quad (3)$$

For the 10-60 MHz HBC channel, we calculated the instantaneous FDTD estimated path loss in decibels using this method. Due to the difficulties of removing the impacts of the transmitting and receiving antennas in such a close-range communication, the estimated path loss includes their effects. We derived the fitted mean log-distance path loss formula for shadow fading parameters after inserting the slope line in the PL vs distance figures. We calculated S_{dB} by taking the difference between calculated and mean path loss from log-distance path loss curve. When both transmitting and receiving antennas are z-directed, Figure 11 shows the average path loss vs distance for

dipoles 150 mm length and loop antennas 150 mm diameter. When both transmitting and receiving antennas are z-directed, Figure 12 displays the average path loss vs distance for dipoles 40 mm length and loop antennas 40 mm diameter. While both transmitting and receiving antennas are z-directed, Figure 13 compares path loss vs distance between dimensions of 150 mm and 40 mm. Tables I and II demonstrate various fitted values for the individual path loss model for frequencies ranging from 10 to 60 MHz, where both transmitting and receiving antennas in the case of dipole and loop respectively are z-directed.

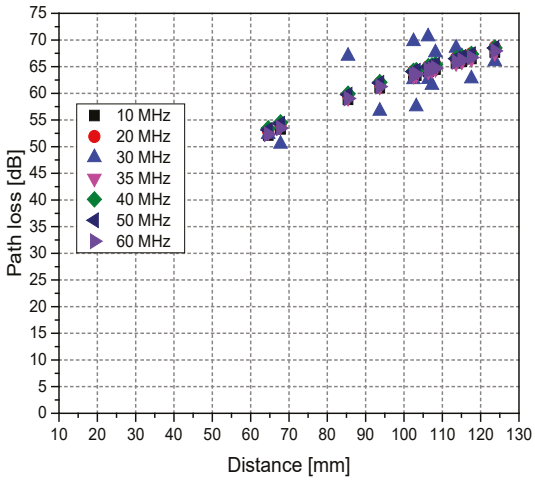

Figure 9
Path loss vs distance for dipole antenna at z-direction

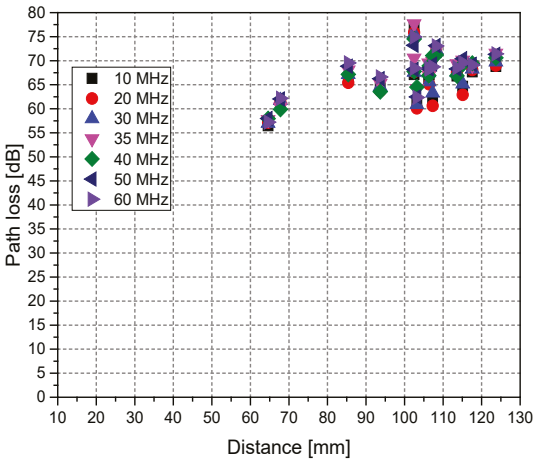

Figure 10
Path loss vs distance for loop antenna at z-direction

Table III shows fitted features of the path loss model expression averaged between 10 and 60 MHz for both the loop and the dipole when the transmitting and receiving antennas are both z-directed.

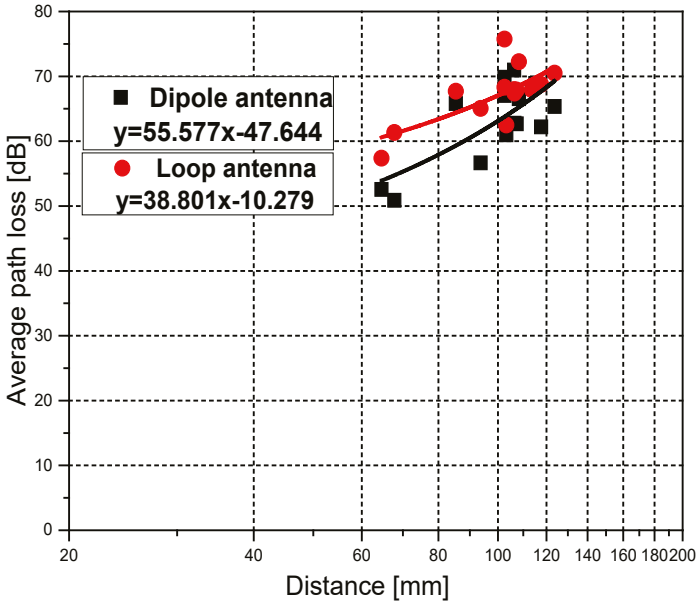

Figure 11

Average PL vs distance for z-directed dipole and loop antennas at 150-mm dimension

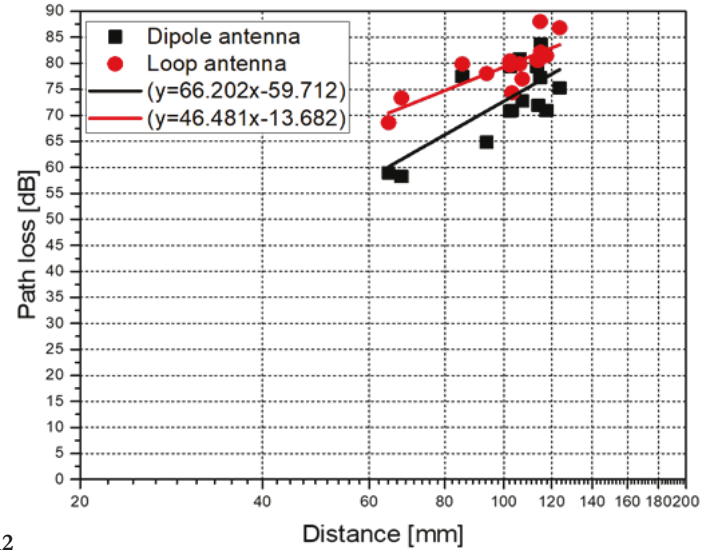

Figure 12

Average PL vs distance for z-directed dipole and loop antennas at 40-mm dimension

Table I.

Fitted factors of path loss model expression at z-direction for dipole antenna

Frequency [MHz]	n	PL_o[dB]	do[mm]	σ[dB]
10	5.52	8.13	10	4.10
20	5.59	7.34	10	4.25
30	5.45	8.48	10	4.29
35	5.25	10.05	10	4.13
40	5.22	10.65	10	3.91
50	5.45	9.02	10	3.95
60	5.54	7.44	10	3.99

Table II

Fitted parameters for path loss model expression at z-direction for loop antenna

Frequency [MHz]	n	PL_o[dB]	do[mm]	σ[dB]
10	3.32	32.71	10	4.00
20	3.15	34.13	10	4.09
30	3.35	32.87	10	3.67
35	4.47	23.49	10	3.18
40	4.27	24.69	10	2.63
50	3.89	28.94	10	2.68
60	3.92	28.28	10	3.07

Table III

Fitted parameters for 10-60 MHz average path loss model expression when both transmitting and receiving antennas are z-directed

Antenna type	n	PL_o[dB]	do[mm]	σ[dB]
Dipole	5.56	7.93	10	3.98
Loop	3.88	28.52	10	3.07

For dipole antennas, the path loss exponent n was 5.56 when the transmitting and receiving antennas were aligned along the body height direction (Haque, Yamada, Shi, Wang, & Anzai, 2021). During the study of "loop antennas, the path loss exponent n was a value of 3.88 while the transmitting and receiving antennas" (Haque, Yamada, Shi, Wang, & Anzai, 2021) were also along the body height direction. Therefore, the loop antenna is showing the lower path loss exponent n in this research in case of z-direction. But when considering all the three directions for the receiving antenna, the path loss does not attenuate significantly with distance for both dipole and loop antenna.

Additionally, MATLAB was used to process the simulated data sets in order to perceive CDF (cumulative distribution function) versus shadow

fading, which is depicted in Figures 14 and 15 correspondingly (Haque, Wang, & Anzai, 2019). The traditional second-order "Aaike information criterion (AIC) test" (Akaike, 1973) was employed to investigate the statistical distribution of the fading term. Normal, log-normal, Rayleigh, Rice, and Weibull distributions are the most common candidates. Using adequate numbers of simulated random numbers, the parameters of the various distributions were estimated using the "maximum likelihood estimation technique" (Haque, Wang, & Anzai, 2019). When the T_x and R_x are both in the z direction, the shadowing statistical distribution in decibels was shown to be a good approximation using normal distribution. As a result, the lognormal distribution appropriately fits shadowing statistics from in-body to on-body (IB2OB). The standard deviation indicates how near the path loss is to its average value and how strong the shadow fading is. Because of lower frequencies from 10-60 MHz, the standard deviation and path loss exponent are less varied in the z direction in our simulation.

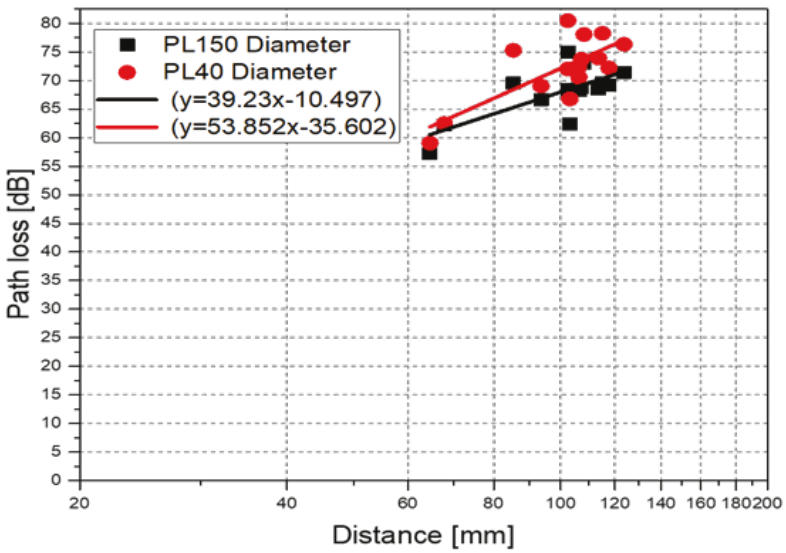

Figure 13

Comparison of average PL vs distance between the sizes of 150-mm and 40-mm antenna

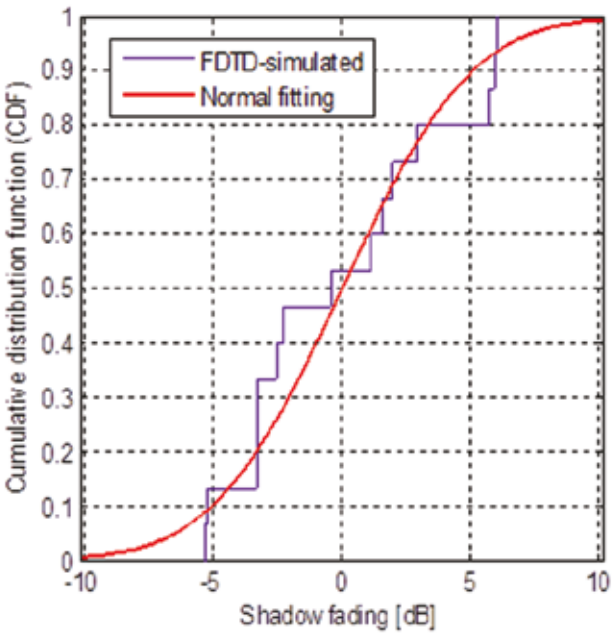

Figure 14
CDF vs shadow fading for dipole antenna at z-direction

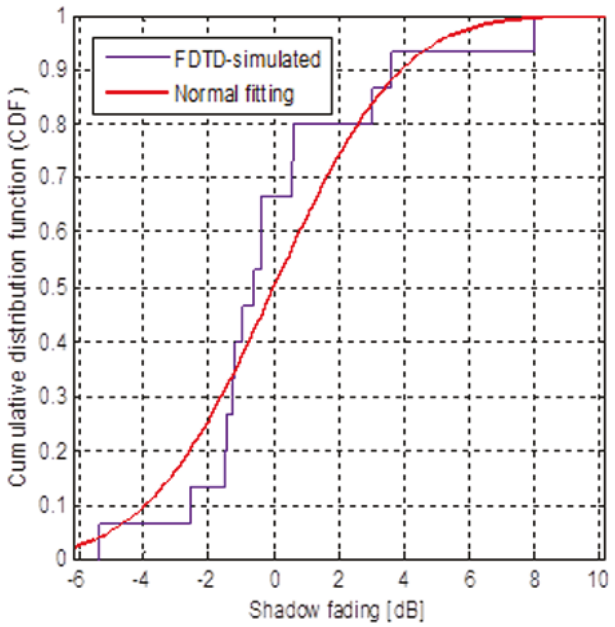

Figure 15
CDF vs shadow fading for loop antenna at z-direction

Consequently, the small path loss values' variance is low because of the human body's weak shadowing effect which is our crucial phenomena.

4. Group delay calculation results and discussion

For group delay, we executed FDTD simulation also by using the anatomical human body model, but a wide band pulse excitation signal by a center frequency at 35 MHz as well as the bandwidth of 50 MHz. From the FDTD simulation, we got time domain waveform of T_x and R_x. To extract the transfer function of the implant communication channel, FFT (Fast Fourier transform) is done in practice from time domain data to frequency domain. Using an FFT analysis, we discovered voltage versus frequency and current versus frequency spectrum of T_x and R_x for dipole and loop antenna respectively. We used the following group delay formula;

$$\tau_g = -\frac{d\varphi}{d\omega} \qquad (4)$$

where φ is the transfer function's phase of the channel in radians, and ω is the angular frequency in rad/s.

Finally, the average group delay in terms of frequency and distance was calculated using the phase spectrum of the transfer function between antennas for transmitting and receiving, as shown in Figures 16 and 17, respectively. The power delay profile of this channel nearly does not spread, and the influence of time delay is very negligible, assuming a data rate of 20 Mbps for "implant communication and a group delay" of roughly 1 ns (Haque, Wang, & Anzai, 2019).

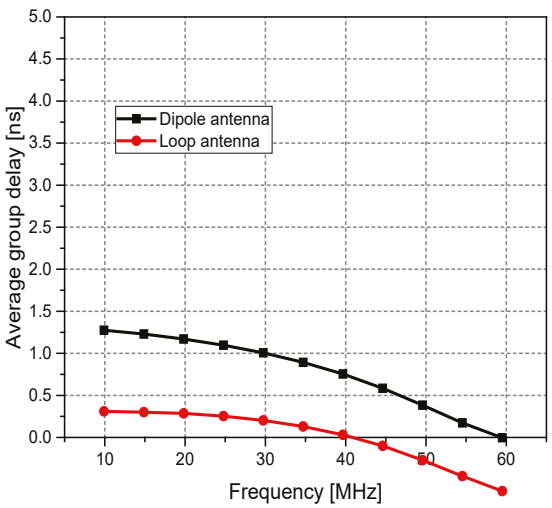

Figure 16

Average vs frequency at about 100 mm distance

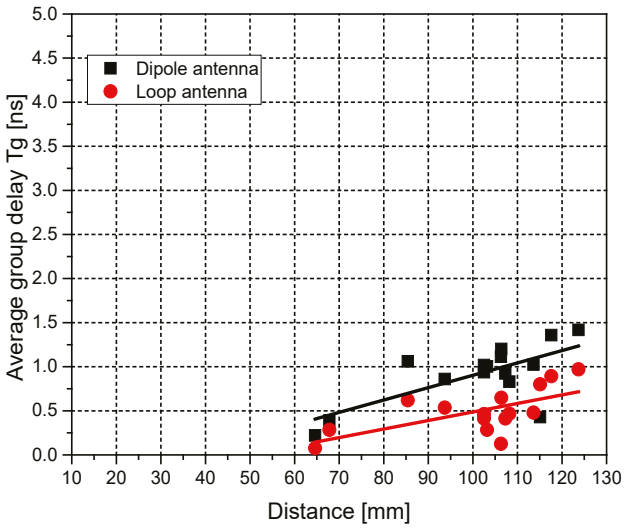

Figure 17
Average τ_g *VS distance*

Some earlier research from our team is connected to the information in this work. In (Shinoda, Anzai, & Wang, 2017; Shi, Anzai, & Wang, 2012; Nagaoka, Watanabe, Saurai, Kunieda, Watanabe, Taki, & Yamanaka, 2004), the authors discussed path loss and group delay in the HBC (human body communication) based on wearable device for employing appropriate channel modeling, communication systems and EMC (Electromagnetic Compatibility). This idea is quite attractive but the range of path loss exponent and group delay has some problems in its adjustable range and accuracy, which makes it limited for applications.

We conducted FDTD simulations for evaluation and the result indicated that our design can work better in reducing the interference of bio-signal transmission. The difference between our work and previous work is summarized into Table IV. A part of our work could be considered as an expansion of previous work, like solving the remained problem about comparing to the path loss exponent n and group delay with a better approach. Our approach is novel that incorporates new technology and applies this concept to the human body area network.

Table IV
Difference between our work and existing work

Parameter	Range of n	[ns]
Existing work	5.59~7.9	1.87
This work	4.65~6.62	0.92

5. Conclusions

Group delay and in-body to on-body path loss must be considered when developing a channel model for in-body to on-body implant communication. Based on a well-defined channel model, we may create an appropriate transceiver structure and optimize communication performance. Using a tiny dipole and loop antenna, we evaluated the propagation properties of an implant channel operating in the 10-60 MHz HBC band. The simulations were carried out using an anatomical human body model and FDTD. For the 10-60 MHz HBC band, it has been discovered that the path loss model expression has path loss exponents of 6.62 and 4.65 and shadowing standard deviations of 3.98 and 3.07, respectively when a small dipole and loop antennas were used for transmitting and receiving along the height direction of the body. The group delays for a small dipole and loop antenna were found to be around 1 ns and less than 1 ns, respectively, which has less impact on data rates below 20 Mbps. Both antennas are good, but the loop antenna is more effective than the dipole antenna, according to the data rate.

This study shows a robust channel model for future wireless medical devices which exploits the advantages of HBC band. Its experimental verification is our future subject.

References

Akaike, H. (1973). *Information theory as an extension of the maximum likelihood principle*. Proceedings of the 2nd international information theory symposium, 267-281.

Anzai, D., Katsu, K., Chavez-Santiago, R., Wang, Q., Plettemeier, D., &Wang, J. (2014). Experimental evaluation of implant UWB-IR transmission with living animal for body area networks. *IEEE Trans. Microwave Theory Tech., 62*(1), 183-192. doi: 10.1109/TMTT.2013.2291542

Gabriel, C. (1996). *Compilation of the dielectric properties of body tissues at RF and microwave frequencies Tech. Rep. AL/OE-TR-1996-0037*. Texas: Brooks Air Force.

Haque, M. I., Wang, J., & Anzai, D. (2019, December 13). *Path loss and group delay analysis at 10-60 MHz human body communication band.* Paper presented at the Institute of Electronics, Information and Communication Engineers (IEICE) conference, *IEICE-119(IEICE-EMCJ-338)*, (pp. 19-23).

Haque, M. I., Yamada, R., Shi, J., Wang, J., & Anzai, D. (2021). Channel characteristics and link budget analysis for 10-60 MHz band implant communication. *IEICE Transactions on Communications, 104*(4), 410-418. doi: 10.1587/TRANSCOM.2020EBP3075

Haque, M. I., Yamamoto, R., Wang, J., & Kakimoto, K. (2022, February 26-27). *Measurement performance of NKN piezo material for powering shoe-mounted sensor*. Paper presented at the 3rd International Conference on Innovations in Science, Engineering and Technology (ICISET-2022), IEEE, Chittagong, Bangladesh. doi: 10.1109/ICISET54810.2022.9775861

Haque, M. I., Yoshibayashi, K., Wang, J., Fischer, G., & Kirchner, J. (2021). Design and evaluation of directional antenna for shoe-mounted sensor for position identification of elderly wanderer. *Sensing and Bio-Sensing Research, 34*, 100451. doi: 10.1016/j.sbsr.2021.100451

Lopez-Linares Roman, K., Vermeeren, G., Thielens, A., Joseph, W., & Martens, L. (2014). Characterization of path loss and absorption for a wireless radio frequency link between an in-body endoscopy capsule and a receiver outside the body. *EURASIP Journal on Wireless Communications and Networking, 2014,* 1-10. doi: 10.1186/1687-1499-2014-21

Nagaoka, T., Watanabe, S., Sakurai, K., Kunieda, E., Watanabe, S., Taki, M., & Yamanaka, Y. (2003). Development of realistic high-resolution whole-body voxel models of Japanese adult males and females of average height and weight, and application of models to radio-frequency electromagnetic-field dosimetry. *Physics in Medicine & Biology, 49*(1), 1.

Peng, Y., Saito, K., & Ito, K. (2018). Antenna design for impulse radio-based wireless capsule endoscope communication systems. *IEEE Trans. Antennas and Propagation, 66*(10), 5031-5042. doi: 10.1109/TAP.2018.2854360

Shi, J., Anzai, D., & Wang, J. (2012). Channel modeling and performance analysis of diversity reception for implant UWB wireless link. *IEICE Transactions on Communications, 95*(10), 3197-3205. doi:10.1587/transcom. E95. B.3197

Shinoda, H., Anzai, D., & Wang, J. (2017). A study on propagation characteristics and transmission performances for 920 MHZ implant communications. *IEICE Tech. Rep., 117*(123), 45-49.

Wang, J. (2020). Wide band human body communication technology for wearable and implantable robot control. *IEICE Transactions on Communications, E103-B*(6), 628-636. doi: 10.1587/transcom.2019HMI0001

Wang, J., & Wang, Q. (2012). *Body area communications: channel modeling, communication systems, and EMC*. Singapore: John Wiley & Sons.

Wang, J., Liu, J., Suguri, K., & Anzai, D. (2015). An in-body impulse radio transceiver with implant antenna miniaturization at 30 MHz. *IEEE Microwave and Wireless Components Letters, 25*(7), 484-486. doi: 10.1109/LMWC.2015.2429112

Wang, J., Nomura, K., Narita, H., Ito, F., Anzai, D., & Bergsland, J. (2018). Development and in vivo performance evaluation of 10–60-MHz band impulse-radio-based transceiver for deep implantation having 10 Mb/s. *IEEE Trans. Microw. Theory Techn., 66*(9), 4252-4260. doi: 10.1109/TMTT.2018.2854165

Yuce, M. R., & Dissanayake, T. (2012). Easy-to-swallow wireless telemetry. *IEEE Microwave Magazine., 13*(6), 90-101. doi:10.1109/MMM.2012.2205833

Corresponding author
Md. Ismail Haque can be contacted at: m.haque.379@nitech.jp